



SEISMIC PERFORMANCE OF ROCKING BUILDING CONTENTS

S.A. Linde⁽¹⁾, D. Konstantinidis⁽²⁾, M.J. Tait⁽³⁾

⁽¹⁾ Graduate Student, Department of Civil Engineering, McMaster University, lindesa@mcmaster.ca

⁽²⁾ Assistant Professor, Department of Civil Engineering, McMaster University, konstant@mcmaster.ca

⁽³⁾ Professor, Department of Civil Engineering, McMaster University, taitm@mcmaster.ca

Abstract

This paper investigates the rocking response of rigid contents in a hospital building. While the rocking response of rigid blocks has been studied extensively, a comparison of contents rocking throughout a building has never been examined. First a four story SCBF was designed and subjected to 20 ground motions at the DBE level. Both the horizontal and vertical floor accelerations were recorded at various locations on each story. These floor accelerations were then used to determine the rocking responses of a variety of different size and slenderness blocks. The effect of the vertical component on the rocking response was examined and found to be insignificant. This means that the location of an object within a given story does not affect its response. The stockier blocks had increasing rocking response higher up the building as expected due to the larger accelerations. However, this result was less distinct for mid-slenderness blocks. Interestingly, for slender blocks the content's height within the building had little effect on its rocking response.

Keywords: rocking; overturning; nonstructural components



1. Introduction

The majority of the overall economic and life loss during most earthquakes can be attributed to the damage and failure of non-structural components and contents [1]. Non-structural components are anything that is not included in the structural system of the building. It includes everything from ceiling tiles and sprinkler systems to the actual contents of the building such as equipment and furniture. These non-structural components and contents comprise at least 80% of the total cost of a building [2]. After a seismic event a building may be structurally sound but the failure of nonstructural contents can render it unusable or even necessitate its demolition. Also, failure of nonstructural components can occur at lower levels of shaking than structural damage and can lead to extensive downtime in essential facilities that are often at their greatest demand immediately following an earthquake [2].

One of the factors inhibiting the seismic design of building contents is that predicting their damage is very difficult because during an earthquake they can slide, twist, rock, bounce, impact walls or other objects, or even overturn [3]. However, understanding the response of these components is critical to making better decisions during the design process to prevent failure. Freestanding slender objects are prone to rocking. Rocking can lead to high internal accelerations that develop upon impact at the base, or even overturning, potentially resulting in damage or safety hazards [3].

The rocking response of rigid objects has been studied extensively since Housner's seminal paper [4] on the subject. These studies have been conducted using sinusoidal pulses, Ricker wavelets, and recorded ground excitations for items such as classical columns, electrical equipment, and art objects. However, the rocking response of an object located at some floor level in a building is very different from that on the ground. Moreover, the vertical base acceleration is rarely considered. Past studies that did include the vertical component have reported varying conclusions concerning its significance. Makris and Zhang [5] showed that including the vertical component has negligible effect on the scaling factor required for a horizontal acceleration record to overturn a given block. In this study the vertical component was scaled with the same factor as the horizontal component. Yim et al. [6] found that inclusion of the vertical accelerations do significantly affect the rocking response but not in a predictable pattern. Dimentberg et al. [7] concluded that the presence of vertical motion, at a scale of 50% of the horizontal motion, increases the overturning probability by 30 – 40%. Shi et al. [8] found that the vertical component did affect the response at various levels of ground excitation but not significantly.

This paper investigates the rocking response of equipment and contents in a four-story hospital building. The rocking response of various contents is determined following a two-stage cascading analysis approach. In the first stage, a suite of 20 ground motions is selected and used to carry out nonlinear time history analysis of a 3D model of the building in OpenSees [9]. This analysis produces floor motions, which are then used in the second analysis stage as input to determine the planar rocking response of contents of different size and slenderness throughout the building. The rocking response of contents placed at various locations on each floor, where they are subjected to different vertical accelerations, is investigated. The rocking response of contents located at different stories is also evaluated and the effect of the content's height within the building is determined.

2. Building Design

The hospital building assumed for the purpose of this study is located in Los Angeles (34.0°N, 118.2°W) and was designed as an essential facility on site class C soil with an S_{DS} and S_{D1} of 1.23 and 0.56 [10]. The hospital is six bays of seven meters in the one direction and four eight meter bays in the orthogonal direction for a total footprint of 1344 m². All four stories are 4.5 m high. It was designed as a special concentrically braced frame (SCBF) in accordance with ASCE 7-10 [11]. The steel members were designed in compliance with AISC 2010 [12]. Fig. 1 shows elevation and plan views of the one bay frame that was modeled in this study.

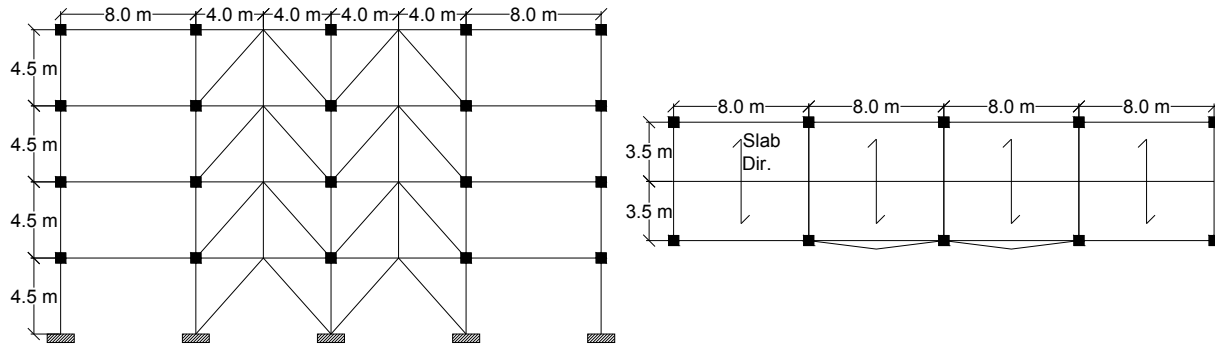


Fig. 1 – Left: Elevation view of SCBF. Right: Plan view of modeled bay

The LFRS consisted of HSS bracing in the center two exterior bays of all four sides. The chevron bracing was designed using the equivalent lateral force procedure with a force reduction factor of 6. Chevron bracing can lead to a soft story formation (excessive drift concentration at one story) when the compression brace buckles if the beam forms a plastic hinge at the brace connection point. Zipper columns were used to avoid the need for excessively large beams to prevent this issue. These columns were designed according to the static design method provided by Kim et al. [13].

A one way slab orientated in the direction of the 3.5 meter span (see Fig. 1) was used at each story. Double span slabs were used making it appropriate to model one full bay width. A ribbed composite steel deck was used with 18 gauge steel decking and a 125 mm thick concrete slab. All the floors were assumed to be equally loaded with a dead load of 4.0 kPa and a live load of 2.5 kPa. A cladding load of 0.96 kPa was also applied to the exterior.

3. Structural Model

A 3D model of one bay width of this hospital was created in OpenSees [9]. The frame was modeled using the expected properties of the members and their materials. The gravity loads were applied as static loads on the column nodes and were taken as the force of gravity acting on the mass tributary to the respective columns. The rest of the gravity load for each story was applied on a leaning column. The leaning column was included to account for P-delta effects.

The seismic mass applied to the frame was taken as the mass attributed to the full dead and live gravity loads. Since the building only has braced frames located at the exterior of the building half the horizontal mass of the building was tributary to each braced frame. The mass on the slab was applied as a mass density and acted in all translational directions. The mass due to cladding was applied in the horizontal and vertical directions to the exterior column nodes. The remainder of the horizontal mass was lumped at each story on the leaning column. The unbraced frame columns also had their tributary vertical mass of the half bay width not modeled applied at each story. Fig. 2 shows the distribution of the mass on the frame typical to each story.

All the members except the braces were structural W-sections and modeled using force-based nonlinearBeamColumn elements. These elements use distributed plasticity and are comprised of fiber sections with 16 fibers along the length of the web and flanges and 4 fibers across them. The steel was modeled using the uniaxial isotropic Steel02 material with the expected yield strength of $f_{y,e} = 379$ MPa, 3% strain hardening, and the other parameters as recommended by OpenSees [9]. The torsional stiffnesses of the beams and columns were then aggregated to the fiber sections.

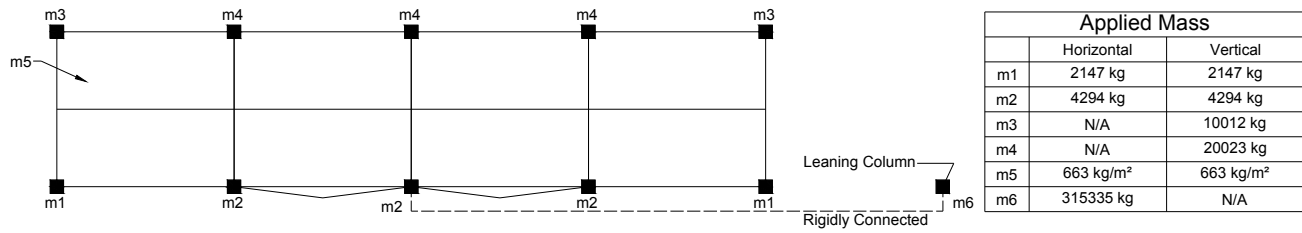


Fig. 2 – Floor mass distribution

All columns used a single element with seven integration points for each story level. The beams, girders, and joists were made up of 8 elements each using 2 integration points. P-delta and linear geometric transformations were used for the columns and the other gravity frame members respectively. The girders, beams and joists were fixed to the slab along their entire lengths. The beams in the braced frame plane were allowed to rotate independently of the slab at the columns. The leaning column was modeled using elastic BeamColumn elements with a large area and low moment of inertia. This allowed the column to take the large axial loads but not provide any additional lateral stiffness. The leaning column nodes were connected to the center column of the braced frame using similar elastic elements.

A different square HSS section was used for the braces at each level of the building. The same material was used as for the other members except the expected yield strength was 345 MPa. The braces were given an initial camber of L/500 (12 mm) at the center by aligning their elements along a half sinusoidal curve. Each brace was comprised of 6 elements with the center four elements being L/16 in length to accurately capture the buckling expected at the middle of the brace. The braces were modeled using force based nonlinearBeamColumn elements with seven integration points and a corotational geometric transformation. Both the flanges and webs were divided into 16 fibers along their length and 4 fibers across their thickness. The braces were fixed to the column and mid-beam nodes in the translational and out of plane rotational degrees of freedom. The in plane rotation was modeled as a gusset plate according the moment-rotation relation given by Hsiao et al. [14] using a zero length rotational spring element. The braces were constrained to buckle entirely in the braced frame plane.

The slab was modeled in OpenSees using ShellMITC4 elements. This is a quadrilateral bilinear isoparametric shell element with modified shear interpolation that gives an accurate thin plate bending response [9]. The slab was divided into meter by meter square elements using 8 and 32 elements in the out of plane direction and in plane directions respectively. The slab was fixed in the translational degrees of freedom at every column but allowed to rotate freely. The composite deck was modeled using an elastic orthotropic material with a constant thickness. The material properties and thickness of the shell element were selected to match the orthotropic properties of the corrugated composite deck slab using the equivalent orthotropic material modeling method. This method works by equating the bending stiffness of the actual slab to that of the model in the longitudinal and perpendicular directions as well as the axial stiffnesses in the longitudinal direction and the shear stiffnesses in the slab’s plane. These conditions are shown in Eq. (1) [15]. The stiffnesses were calculated in accordance with ANSI/SDI C-2011 using the cracked concrete section properties (ANSI 2012). The poisson’s ratios are taken as zero which neglects the coupled effects in different directions and is consistent with literature for cracked concrete [16, 17]. The out of plane elastic modulus, E_y , and the two out of plane shear modulus’s, G_{xy} and G_{yz} , are taken as relatively small in relation to the other directions [15]. The four equations are solved for the four unknowns; d , E_z , E_x , and G_{xz} . The depth of the slab was taken as 129 mm and the equivalent orthotropic material properties are shown in Table 1.

$$E_z \frac{bd^3}{12} = E_c I_{cr,z}; E_x \frac{bd^3}{12} = E_c I_{cr,x}; E_z bd = EA; G_{xz} d = Gt \quad (1)$$

where: Z – Parallel to ribs; X – Perpendicular to ribs; Y – Vertical direction

The bases of all ten columns were fully fixed in all 6 degrees of freedom. The entire plane containing the unbraced frame was also constrained in the out of plane direction to ensure the frame only responded in horizontal direction of excitation and vertically. The leaning column was also constrained against motion in the



out-of-plane direction. In order to avoid torsion in the frame, because only one side is braced, the rotational, in-plane horizontal, and vertical translational degrees of freedom of the corresponding columns nodes in each plane were equated at each level.

Table 1 – Orthotropic Material Properties for Composite Steel Deck Slab

Elastic Modulus	Shear Modulus
$E_x = 6.53$ GPa	$G_{xy} = 0.75$ GPa
$E_y = 1.73$ GPa	$G_{xz} = 2.51$ GPa
$E_z = 8.57$ GPa	$G_{yz} = 0.75$ GPa

Five percent Rayleigh damping in the superstructure was applied at the first vertical and horizontal modes. The stiffness matrix in the calculation of the damping coefficients was taken at the last committed state determination. The Krylov-Newton algorithm was used in OpenSees. If this was unable to attain convergence at any time step various other algorithms were tried. The time step used in analysis was taken as a tenth of the time step of the ground motion record. This small time step was used to minimize fictitious spikes in the floor acceleration due to system nonlinearities. This phenomenon has been noted previously [18] and it has been shown that spikes are due to physical phenomena but can be overestimated due to numeric modeling assumptions. These exaggerated floor acceleration spikes occurred in the SCBF when the braces first buckle in compression and have been nearly eliminated by the use of the small time step.

The periods of the modeled frame as calculated using elastic eigenvalue analysis are shown in Table 2. Horizontal modes are determined as modes that react primarily in the lateral direction and are in very close to the periods and mode shapes of an eigenvalue analysis using only horizontally activated mass. The first 12 modes are full bay by full bay deflections of the slabs. The first period of the slab is somewhat large at 0.6 seconds but this is due to using the mass accredited to the full dead and live loads and the cracked section properties of the slab. The primary horizontal period of the building is 0.46 s which is close to the code predicted period of 0.43 s [17].

Table 2 – Period Values of the SCBF

Horizontal		Vertical	
Period Value	Mode	Period Values	Modes
0.46 s	13	0.60 – 0.47s	1 - 12
0.21 s	38	0.41 – 0.22 s	14 - 37
0.13 s	74	0.21 – 0.15 s	39 - 73

4. Ground Motion Selection and Scaling

A suite of 20 ground motions was selected for the time history analysis. All the records were selected from Baker’s broadband suite set 1a [19]. This suite consists of 40 unscaled ground motions, all of which include fault normal, fault parallel and vertical components. Baker selected these motions to match the target spectrum and log variance predicted by Boore and Atkinson’s ground motion prediction equation [20] for a magnitude 7 strike-slip earthquake at 10 km on a soil site [19]. The site location had a soil class C ($v_{s30} = 365 - 760$ m/s) while the earthquakes selected had shear wave velocities from 200 – 400 m/s. A disaggregation of the seismic hazard at the hospital site for the spectral period of the fixed base building shows that the vast majority of the

contribution is from magnitude 6.5 – 7.5 earthquakes at 5 – 15 km [21]. Overall, this makes Baker’s set 1a an ideal suite to select ground motions for time history analysis from.

The individual response spectra for all 80 horizontal ground motion components were then computed and scaled to the design spectrum to minimize the sum of the square of the difference between them over a period range of 0 to 4 seconds. The twenty horizontal components with the least minimum residual error were selected for time history analysis. A maximum of one horizontal component per record was used. Although this is not the preferred scaling procedure it does provide a close match at the fixed base period and was done for the sake of a future publication which will compare the results of this paper with the rocking response of contents in base-isolated buildings with periods in the 2.5 – 4 second range. The horizontal response spectra of the resulting suite including the mean and design spectrum are shown in Fig. 3 (left). The vertical components were scaled with the same factor as the corresponding horizontal components. The vertical response spectra are shown in Fig. 3 (right).

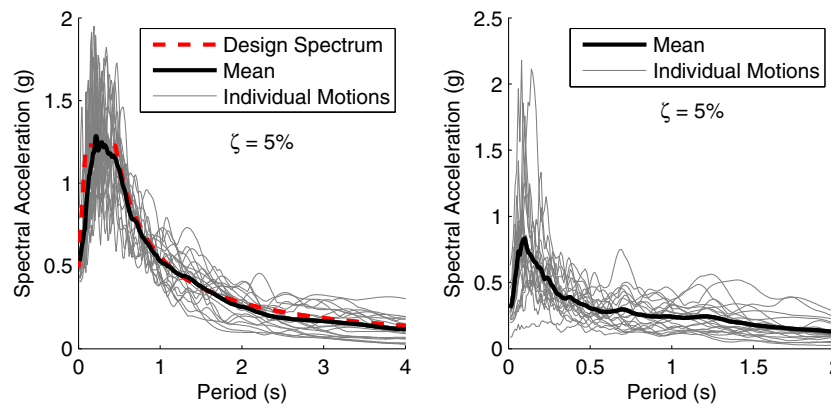


Fig. 3 – Scaled ground response spectra for 20 selected earthquakes. Left: horizontal spectra. Right: vertical spectra.

5. Building Response

The 20 ground motions were then used to determine the floor accelerations at various locations on each level. The vertical accelerations in the unbraced bays were found to be the most critical and thus these locations were examined in following analysis. Fig. 4 shows a floor plan of the one bay width that was modeled depicting the 5 locations where the accelerations were recorded.

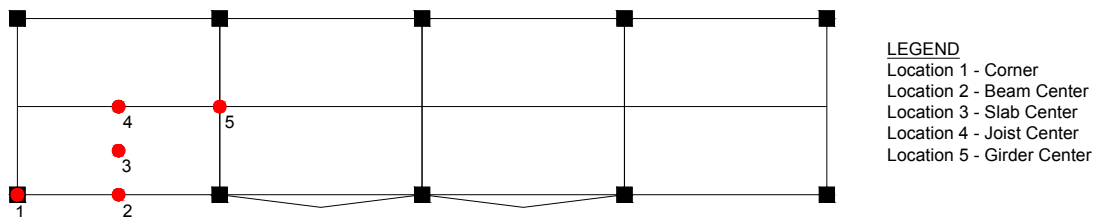


Fig. 4 – Floor locations where the acceleration time histories were recorded

Fig. 5 shows the average responses of the frame for the 20 ground motions. The average maximum interstory drift was largest between the second and third stories. The second story braces buckled first in the majority of the analysis leading to larger interstory drifts. However, the zipper columns prevented excessive drift from accumulating at this level and assisted in distributing the ductility demand to the first and third stories. The average horizontal peak absolute floor velocity increases nearly linearly with building height from an average of 0.55 m/s at the ground to 1.01 m/s at the roof. The average absolute peak floor acceleration also increases with building height to a maximum of 10.2 m/s² at the roof. The average peak vertical accelerations increase with

building height as well. The center of the bay (location 4) had the largest peak vertical acceleration at each story level followed by the center of the slab (location 3), the midspan of the beams in either direction (locations 2 and 5), and the corner (location 1). This distribution was expected based on the primary vertical mode shape.

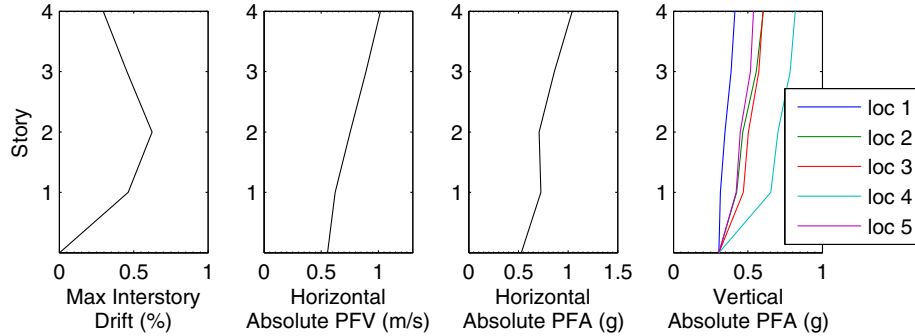


Fig. 5 – Average building responses

The average horizontal floor spectra for each floor are shown in Fig. 6 (left). The peaks are located at a slightly longer period than the natural period, 0.46 s, due to period elongation from yielding. Fig. 6 (right) shows the vertical response spectra at the roof for the various floor locations. The spectra at the other stories have the same shapes with lower spectral accelerations. Locations 3, 4, and 5 have peaks at the primary vertical periods, 0.6s. However, all the locations have a higher spectral acceleration at around 0.1s which corresponds to the average peak spectral acceleration of the vertical component of the ground excitations.

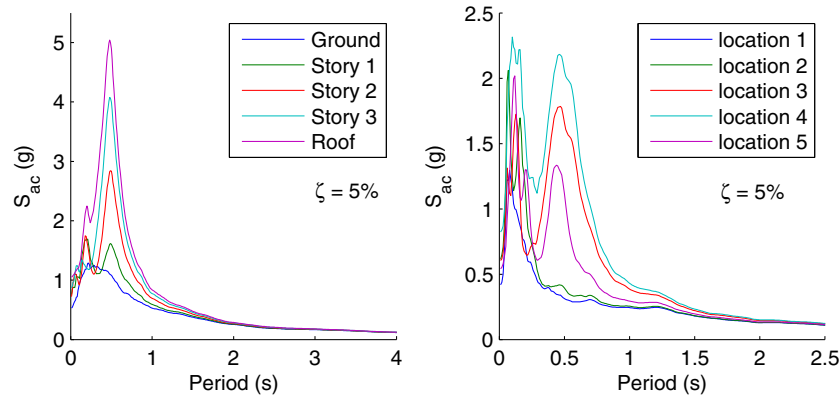


Fig. 6 – Left: Horizontal floor response spectra at each story. Right: Vertical floor response spectra at various locations on the roof

6. Response of Rocking Contents

The nonstructural contents under consideration in this paper are treated as rigid objects. This assumption was shown to be accurate by Konstantinidis and Makris [22] during shake-table tests of various types of laboratory equipment. Fig. 7 shows a rocking rigid object with slenderness $\alpha = \tan^{-1}(b/h)$ and frequency parameter $p = \sqrt{3g/4R}$, where $R = \sqrt{h^2 + b^2}$, in planar rocking motion. The equation of motion of the rocking block is [6],

$$\ddot{\theta} = -p^2 \left\{ \left(\frac{\ddot{U}_b^y}{g} + 1 \right) \sin(\text{sgn}(\theta)\alpha - \theta) + \frac{\ddot{U}_b^x}{g} \cos(\text{sgn}(\theta)\alpha - \theta) \right\} \quad (2)$$

where \ddot{U}_b^x and \ddot{U}_b^y are the horizontal and vertical acceleration, respectively, of the pivot point on the floor; these acceleration histories are determined from the nonlinear time history analysis of the structural model. The

coefficient of restitution, e , which relates the angular velocities immediately before, $\dot{\theta}_1$, and after, $\dot{\theta}_2$, the impact through $e = \dot{\theta}_2 / \dot{\theta}_1$ is used to take into account the energy lost upon impact. The maximum coefficient of restitution, obtained by conservation of angular momentum before and after the impact, is given by [4]:

$$e = 1 - \frac{3}{2} \sin^2 \alpha \quad (3)$$

The equation of motion for the rocking block is solved by integration in Matlab [23] using standard ODE solvers.

The inclusion of vertical base accelerations enables the possibility that the block may lift off of the floor surface on which it is rocking, rendering the rocking equation of motion invalid. In order to detect this potential scenario, the normal force at the rocking edge of the rigid block is determined at every time step. If the normal force becomes negative, the block has lifted off and the analysis is stopped. Any time histories which cause lift off are omitted from the rocking results.

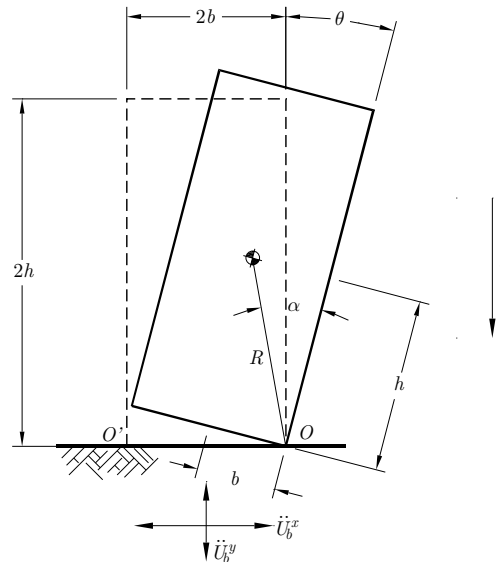


Fig. 7 – Schematic of rocking block (clockwise rotation θ is positive)

6.1 Introduction to rocking spectra and an example response

The rocking time histories were determined for objects on each floor location at all the stories. Rocking time histories were found for 120 different blocks ranging from $R = 7.5 \text{ cm} - 11.9 \text{ m}$ and with slenderness of 10° (e.g. bookcase), 15° (e.g. upright desktop computer), 20° (e.g. 4-drawer filing cabinet). The rocking time histories for a common refrigerator ($2b = 0.6\text{m}$, $2h = 1.8\text{m}$, $\alpha = 18.4^\circ$, $p = 2.8 \text{ rad/s}$) subject to the floor accelerations at the corner of the building under the 1979 Imperial Valley Brawley Airport fault parallel record are shown in Fig. 8. Interestingly, the fridge on the third story overturns, while the fridge on the roof does not. This is a product of the high nonlinearity involved in both the building and rocking responses. Also clearly visible is that the rocking frequency is not constant but depends heavily on the rocking amplitude.

Typically only the maximum value of rotation from the rocking time history is of interest. When many analyses are done with the same time history for many different size and slenderness blocks, the results are often shown as a rocking spectrum [24]. A rocking spectrum plots the maximum angle of rotation (normalized by the slenderness of the block) as a function of the block's size, usually expressed as $2\pi/p$. Different slenderness values are shown as separate lines. The maximum angle of rotation for blocks that tip is taken as α to avoid

skewing the mean when the rocking spectra for the 20 ground motions are averaged out for a given location in the building.

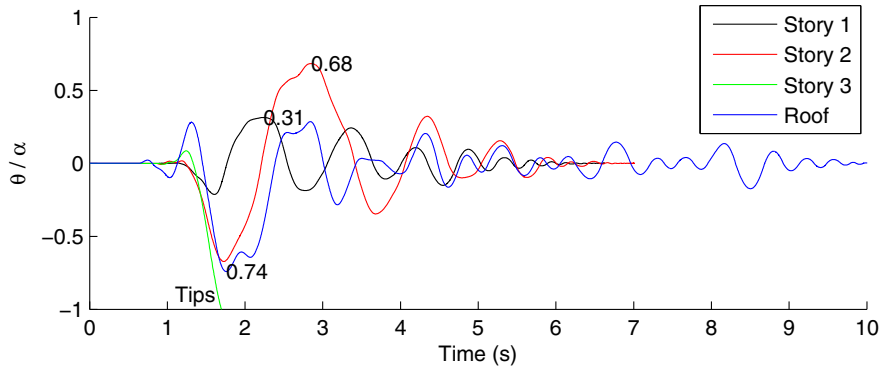


Fig. 8 – Example Rocking Response of a fridge located near a column

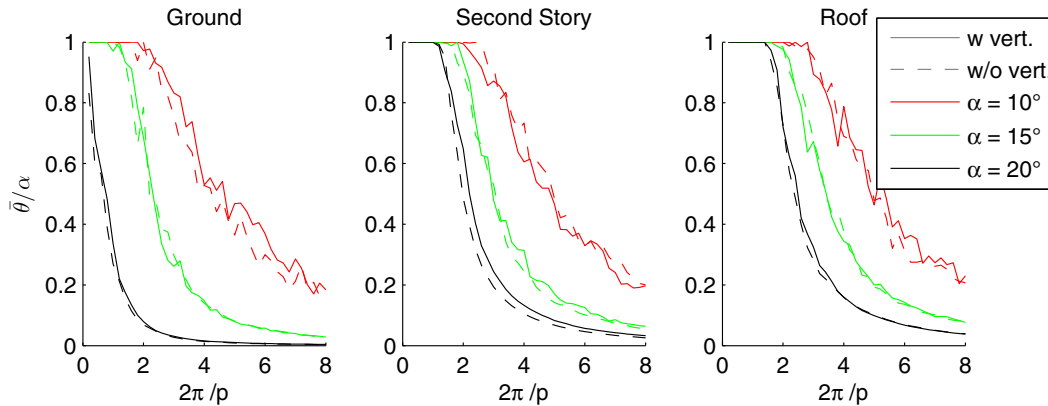


Fig. 9 – Effect of the vertical acceleration component on the rocking response

6.2 Effect of vertical acceleration

One objective of this study was to determine how the vertical floor accelerations contributed to the rocking response. To analyze this effect rocking spectra were created in Matlab using only the horizontal floor accelerations. These were then compared to the original rocking spectra which were calculated using both the horizontal and vertical components. This comparison is shown in Fig. 9 for the rocking spectra at location 4 (center of the joist) for the ground, second story, and the roof. The joist was selected because it had the highest peak vertical floor accelerations as well as the highest vertical floor response spectra as shown in Fig. 5 and Fig. 6. These graphs show that the vertical acceleration has minimal effect on the rocking response regardless of size, slenderness or story. The vertical accelerations at the center of the joist were substantial, even producing lift off in a few cases, and yet did not affect the degree of rocking to which contents underwent. Notably, where there were the highest vertical accelerations, i.e. the roof, there were the highest horizontal accelerations as well which continued to dominate. Where the horizontal accelerations remained the same at a given story and the vertical accelerations increased towards the center of the bay the effect of the vertical acceleration on the rocking response was increased as well.

6.3 Effect of content placement on a particular floor

Fig. 10 shows the average rocking spectra for the 20 ground motions at the roof for the different floor locations. The obvious conclusion is that the location of a block on the floor does not affect its rocking response. The result was similar for the other stories. This is expected from the previous section which showed that vertical

accelerations had minimal effect on the rocking response. The important conclusion is that it is not necessary to know the location of a piece of equipment on a floor level or the vertical accelerations at that level to be able to accurately predict the content's rocking response.

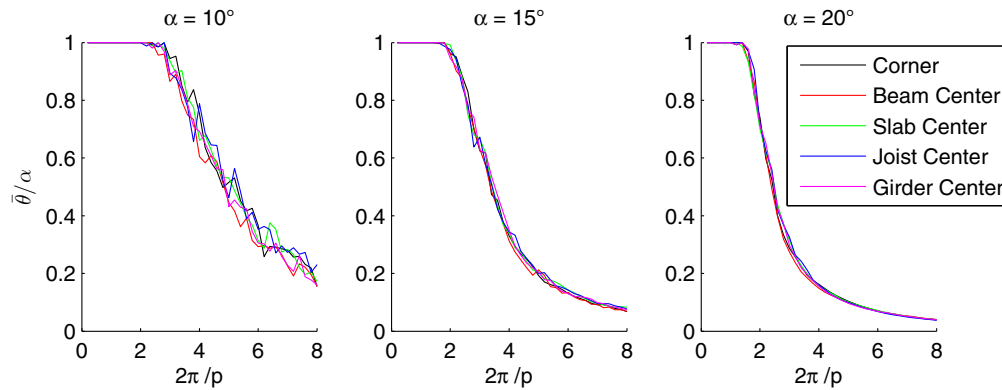


Fig. 10 – Rocking spectra at different locations on the roof

6.4 Effect of floor level

Also of interest is the difference in the rocking response from one story to another. Since the placement on the floor had minimal effect on the rocking spectra, the analysis is continued using the results at the corner of the building. The floor accelerations increase higher up the building which is expected to increase the rocking response. This was the situation for stockier blocks ($\alpha = 20^\circ$) as shown in Fig. 11 (right). The rocking response increased with the story number. The largest difference in response was between the ground and the first story. The difference between adjacent stories decreases up the building ending in minimal difference between the third story and the roof. However, this result becomes less evident as objects become more slender. At a slenderness of 15° the rocking response still increases from one floor to the next but the differences are less pronounced (Fig. 11 center). For slender blocks with $\alpha = 10^\circ$ (Fig. 11 left) the relative height of the content in the building has little impact on the rocking response. This result holds true for each individual motion as well.

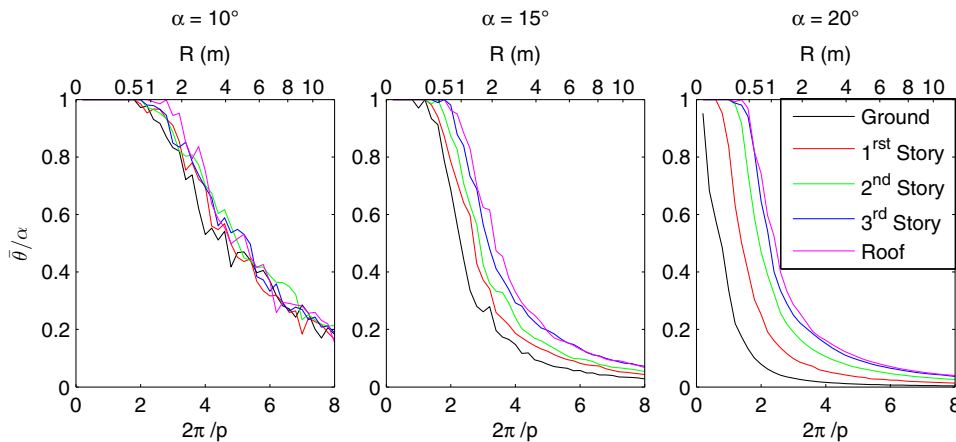


Fig. 11 – Rocking spectra for all stories at the corner

Fig. 12 shows the average maximum angle of rotation plotted against the building height for contents with slenderness $\alpha = 10^\circ, 15^\circ$ and 20° and size $R = 0.5, 1$ and 2 m. This figure confirms the previous conclusion with the slender lines being nearly vertical, i.e. the height of the content within the building has little effect on its rocking motion. Smaller blocks have a large difference between slendernesses at the ground but very similar at the roof. The small stocky blocks had the largest increase in response over the building height. There is a small

difference between the responses of the stocky blocks at the ground but it increases with height whereas for the slender and mid-slender blocks the difference between sizes was fairly uniform over the stories for the sizes plotted.

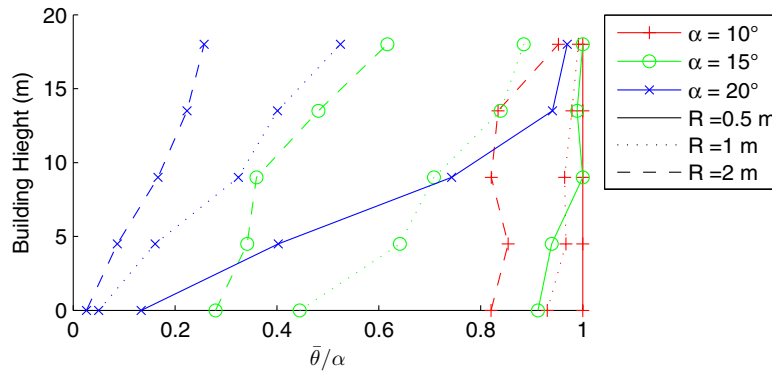


Fig. 12 – Height v. theta for select block sizes

7. Conclusions

This paper examined the rocking response of slender nonstructural building contents. First a 3D OpenSees model of a four-story SCBF hospital was developed and subjected to 20 broadband ground motions. The floor acceleration time histories were computed at different locations on each story. The rocking response of a wide variety of rigid blocks with different size and slenderness was determined using as excitation the floor acceleration histories at each location. The rocking response results were then analyzed and responses between the different locations were compared.

The vertical ground acceleration component was also included to study its effect on the rocking response. This also introduced the ability of the rocking block to lift off the floor. One of the main conclusions of this paper is that even at locations with high vertical acceleration components, such as at the center of the bay on the roof, the effect of the vertical acceleration component on the rocking response is minimal. The consequence of this is that the rocking response does not depend on the location of an object within a story. As expected, the rocking response does increase at higher stories in the building for stocky ($\alpha = 20^\circ$) blocks. However, the difference in the rocking response from one story to the one above it decreased nearer the roof. Smaller stocky blocks experienced larger increases in the rocking response as the content's height in the building increased. Interestingly, for slender blocks ($\alpha = 10^\circ$), the position of the content within the building had little discernable effect on the rocking spectra. For blocks with an intermediate slenderness ($\alpha = 15^\circ$), the content's height mattered but did not have as much effect as for the stocky blocks.

Given the complexity of the rocking problem and the variability in the dynamic characteristics of different structural systems, further studies are needed to develop a better understanding of the seismic response of unanchored slender objects in buildings.

8. Acknowledgements

The authors acknowledge the advice of Dr. F. Nikfar on the modeling of the hospital building in OpenSees.

9. References

- [1] CSA S832-06 (2011): Seismic risk reduction of operational and functional components (OFCs) of buildings. Canadian Standards Association: Mississauga, ON.
- [2] Taghavi S, Miranda E (2003): Response assessment of nonstructural building elements. *Report No. PEER 2003/05*, Pacific Earthquake Engineering Research Center, University of California, Berkeley, CA.



- [3] Konstantinidis D, Makris N (2009): Experimental and analytical studies on the response of freestanding laboratory equipment to earthquake shaking. *Earthquake Engineering and Structural Dynamics*, **38**(6), 827-848.
- [4] Housner GW (1963): The behavior of inverted pendulum structures during earthquakes. *Bulletin of the Seismological Society of America*, **53**, 403–417.
- [5] Makris M, Zhang J (1999): Rocking response and overturning of anchored equipment under seismic excitation. *Report No. PEER 1999/06*. Pacific Earthquake Engineering Research Center, University of California, Berkeley.
- [6] Yim C, Chopra AK, Penzien J (1980): Rocking response of rigid blocks to earthquakes. *Earthquake Engineering and Structural Dynamics*, **8**, 565–587.
- [7] Dimentberg MF, Lin YK, Zhang R. (1993): Toppling of computer-type equipment under base excitation. *Journal of Engineering Mechanics*, 119(1), 145-160.
- [8] Shi B, Anooshehpour A, Zeng Y, Brune JN (1996): Rocking and overturning of precariously balanced rocks by earthquake. *Bulletin of Seismological Society of America*, **86**(5): 1364-71.
- [9] McKenna F, Fenves GL, Scott MH. Open system for earthquake engineering simulation (OpenSees) <http://opensees.berkeley.edu>.
- [10] USGS 2014, U.S. Seismic Design Maps, U.S. Geologic Survey, Reston, VA.
- [11] American Society of Civil Engineers (ASCE). Minimum design loads for buildings and other structures, *ASCE7-10*, Reston, VA, 2010.
- [12] American Institute of Steel Construction (AISC). *AISC 341-10 Seismic Provisions for Structural Steel Buildings*. Chicago, IL, 2010.
- [13] Kim J, Cho C, Lee K, Lee C (2008): Design of zipper column in inverted V braced steel frames. Proceedings of the 14th World Conference on Earthquake Engineering, Beijing, China.
- [14] Hsiao P-C, Lehman DE, Roeder CW (2012): Improved analytical model for special concentrically braced frames. *Journal of Constructional Steel Research*, **73**, 80-94.
- [15] Zhang W, Cai C, Pan F (2013): Finite element modeling of bridges with equivalent orthotropic material method for multi-scale dynamic loads. *Engineering Structures*, 54(9), 82-93.
- [16] Huang Z, Burgess L, Plank R (1999): Nonlinear analysis of reinforced concrete slabs subjected to fire. *ACI Structural Journal*, **96**(1), 127-136.
- [17] Park R, Gamble W (2000): *Reinforced Concrete Slabs, 2nd Ed*. Wiley.
- [18] Wiebe L, Christopoulos C (2010): Characterizing acceleration spikes due to stiffness changes in nonlinear systems. *Earthquake Engineering and Structural Dynamics*, **39**(14), 1653-1670.
- [19] Baker JW, Ling T, Shahi SK, Jayaram N (2011): New ground motion selection procedures and selected motions for the PEER Transportation Research Program, Draft Report, Pacific Earthquake Engineering Research Center, University of California, Berkeley, CA.
- [20] Boore DM, Atkinson GM (2008): Ground-motion prediction equations for the average horizontal component of PGA, PGV, and 5%-damped PSA at spectral periods between 0.01 s and 10.0 s. *Earthquake Spectra*, **24**(1), 99-138.
- [21] USGS (2008): Seismic Hazard Analysis Tools – Interactive Disaggregation. U.S. Geologic Survey, Reston, VA
- [22] Konstantinidis D, Makris, N (2005): Experimental and analytical studies on the seismic response of freestanding and anchored laboratory equipment. *Report No. PEER 2005/07*. Pacific Earthquake Engineering Research Center, University of California, Berkeley.
- [23] MATLAB, 2009. Version R2009a. *The Language of Technical Computing*. The Mathworks, Inc.: Natick, MA.
- [24] Makris N, Konstantinidis D (2001): The rocking spectrum and the shortcomings of design guidelines. *Report No. PEER 2001/07*, Pacific Earthquake Engineering Research Center, University of California, Berkeley, CA, 2001.